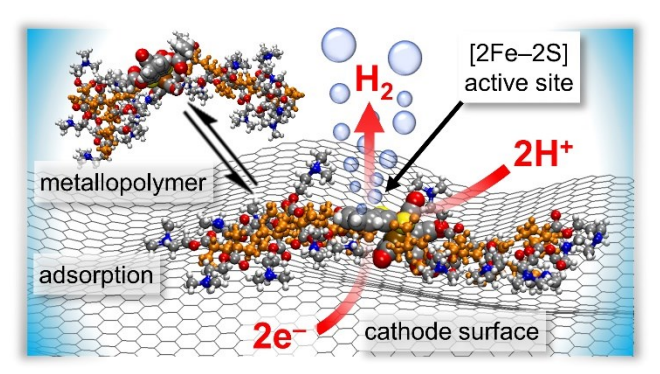
Natural Assembly of Electroactive Metallopolymers on the Electrode Surface: Enhanced Electrocatalytic Production of Hydrogen by [2Fe–2S] Metallopolymers in Neutral Water

Kayla E. Clary[‡], Arthur C. Gibson[‡], Richard S. Glass,* Jeffrey Pyun,* and Dennis L. Lichtenberger*

Department of Chemistry and Biochemistry, The University of Arizona, 1306 East University Boulevard, Tucson, AZ, 85721. USA

KEYWORDS Electrocatalysis Hydrogen Metallopolymers Electrolysis

ABSTRACT: A molecular catalyst attached to an electrode surface can in principle offer the advantages of both homogeneous and heterogeneous catalysis. Unfortunately, some molecular catalysts constrained to a surface lose much or all of their solution performance. In contrast, we have found that when a small molecule [2Fe–2S] catalyst is incorporated into metallopolymers of the form PDMAEMA–g–[2Fe–2S] (PDMAEMA = poly(2-dimethylamino)ethyl methacrylate) and adsorbed to the surface, the observed rate of hydrogen production increases to $k_{\rm obs}$ > 10^5 s⁻¹ per active site with lower overpotential, increased lifetime, and tolerance to oxygen. Herein, the electrocatalytic performances of these metallopolymers with different length pol-



ymer chains are compared to reveal the factors that lead to this high performance. It was anticipated that smaller metallopolymers would have faster rates due to faster electron and proton transfers to more accessible active sites, but the experiments show that the rates of catalysis per active site are largely independent of the polymer size. Molecular dynamics modelling reveals that the high performance is a consequence of adsorption of these metallopolymers on the surface with natural assembly that brings the [2Fe–2S] catalytic sites into close contact with the electrode surface while maintaining exposure of the sites to protons in solution. The assembly is conducive to fast electron transfer, fast proton transfer, and a high rate of catalysis regardless of polymer size. These results offer a guide to enhancing the performance of other electrocatalysts with incorporation into a polymer that provides optimal interaction of the catalyst with the electrode and with solution.

1. INTRODUCTION

Electrocatalysis has a major role in developing efficient energy and chemical conversion processes for a sustainable future.1-4 Perhaps the simplest and most fundamental of these electrocatalytic processes is the reduction of protons to molecular hydrogen by water electrolysis. Unfortunately, the most energy efficient catalysts for the hydrogen evolution reaction (HER) are made from rare and expensive platinum (Pt). Many molecular based electrocatalysts composed of Earth-abundant elements are being developed as alternatives to Pt catalysts.^{5,6} One example is based on the diiron hydrogenase enzyme [2Fe-2S] active site comprised of two of the cheapest and most Earth-abundant elements, iron and sulfur. Small molecule [2Fe-2S] butterfly clusters with structures containing a variety of μ₂-dithiolato moieties and ancillary ligands have shown promise as HER catalysts.^{7–10} However, these [2Fe–2S] small-molecule mimetics generally suffer from water insolubility, short catalyst lifetimes, and oxygen sensitivity.11,12

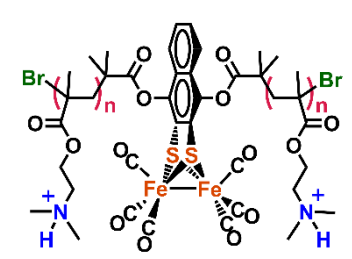


Figure 1. Composition of the PDMAEMA–*g*–[2Fe–2S] metallopolymers in this study, where the polymer length n varies from 9 to 112. When solvated in neutral water, the amine groups on the PDMAEMA polymer catalyst are 91% protonated.

A major advance in the design of [2Fe–2S] catalysts for hydrogen production has been the synthesis of novel water soluble metallopolymers that function as highly active and robust electrocatalysts in neutral water.^{13–15} Like hydrogenase enzymes, these metallopolymers have macromolecular

structures that help to isolate the [2Fe-2S] active site from undesirable side reactions and aid catalytic function. 16 We previously suggested that a polymer corona may serve to isolate the [2Fe-2S] active site from associative degradation reactions encountered in small molecule [2Fe-2S] catalysts. 13,15,17 Other studies have embedded [2Fe-2S] catalysts either covalently or via supramolecular interactions into macromolecular frameworks such as dendrimers, proteins, metalorganic frameworks, and more, but few have retained sufficient catalytic activity. 15 This is not surprising considering an active site embedded in a macromolecule is likely to have inhibited electron and proton transfer. However, we found that a PDMAEMA-g-[2Fe-2S] metallopolymer (Figures 1 and 2, PDMAEMA = poly(2-dimethylamino)ethyl methacrylate) achieves hydrogen evolution rates of >105 s-1 per active site and high catalytic current densities exceeding 100 mA/cm² in the presence of air with 100±3% Faradaic efficiency.¹⁸ This performance is greater than for the small molecule [2Fe-2S] catalysts without the polymer. Furthermore, this system surpasses the rate of diiron hydrogenases19-21 by an order of magnitude and approaches the current densities of platinum electrodes at 0.2 V or less higher overpotential.13

A major unresolved question concerns the role of the polymer support in enhancing the stability while also allowing fast electron and proton transfers for surprisingly fast proton reduction. Previously, we synthesized metallopolymers of various molecular weights from a [2Fe–2S] metalloinitiator containing a propanedithiolate (pdt) bridgehead and a single atom transfer radical polymerization (ATRP) initiation site. The catalytic activity was shown to increase with smaller molecular weights. Unfortunately, the pdt-bridged [2Fe–2S] active site had much poorer catalytic activity than the PDMAEMA–g–[2Fe–2S] system (Scheme 1) and required using pH 4 acidic solution conditions. Additionally, the dependence of electron transfer rates and proton rates on metallopolymer size remained unknown. 22

Herein, we investigate these deeper fundamental questions using a suite of electrochemical and computational methods on metallopolymer catalysts of varying size. The metallopolymers with smaller hydrodynamic radii (R_h) show increased current densities (current per unit electrode area) at lower overpotentials when compared to their larger sized metallopolymer analogues. Impedance spectroscopy and various voltammetry techniques have been employed for the first time on these electrocatalyst systems to quantify the *per-active site* rates of electron transfer and catalysis for these metallopolymers. The *per-active site* rates are found to be similar regardless of the polymer size.

This similarity in per-active site rates is explained by the nature of the adsorption of the metallopolymers to the electrode surface. Computational simulations are used for the first time to reveal the interfacial dynamics between the metallopolymer catalyst and the electrode surface. Snapshots from a molecular dynamics simulation of the structure of the 3.5 kDa metallopolymer in solution and adsorbed on a carbon electrode are shown in Figure 2. The modelling shows that the initial attraction of the metallopolymers to the surface is driven by the electrostatic interaction of the positive protonated amines of the polymer to the negative electric field of the electrode. The metallopolymers self-

assemble on the surface such that, regardless of the polymer size, the catalytically active [2Fe-2S] sites have similar close orientations to the electrode surface for fast electron transfer and similar exposure to solution for fast proton transfer and reduction. The polymers are posited from these simulations to spread themselves into a close-packed monolayer on the electrode surface, and comparison with the experimental measure of the electrochemical surface coverage (ECSC) indicates every adsorbed [2Fe-2S] site in the closepacked arrangement is catalytically active. The dominant factor in the difference in electrocatalytic current density as a function of polymer size is found to be the number of metallopolymers that fit on the surface of the electrode per unit area. The features of the polymer and the surface that lead to this assembly should apply as well to other molecular catalysts embedded in these polymer chains. Thus, these results offer an approach that could improve the performance of other molecular electrocatalysts.

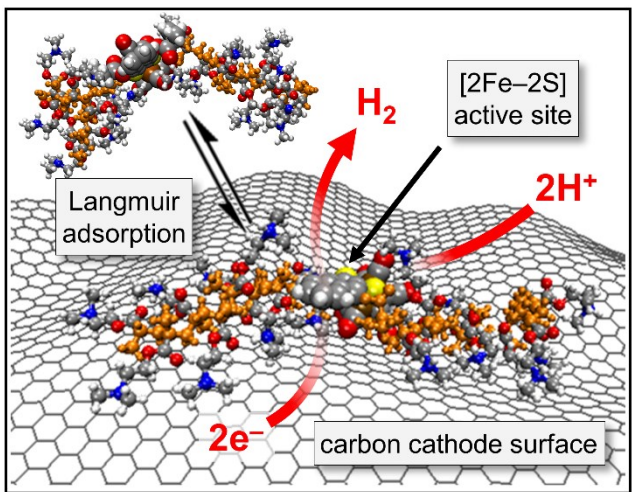


Figure 2. Representative molecular dynamics snapshots of the 35 kDa PDMAEMA-*g*-[2Fe-2S] metallopolymer in solution (upper left) and adsorbed on a graphite surface. The [2Fe-2S] active sites are shown as space-filling spheres between the polypropylene polymer backbone chains (in orange). The DMAEMA units are shown with the protonated amines in blue.

2. RESULTS AND DISCUSSION

Metallopolymer preparation. The preparation of an arbitrary size PDMAEMA-q-[2Fe-2S] metallopolymer **C** (Scheme 1) by ATRP starting from the [2Fe-2S] metalloinitiator molecule A, DMAEMA molecule B, and the Cu(I)Br/HMTETA catalyst has been described previously.¹³ In order to obtain different molecular weight metallopolymer samples, well-controlled ATRP polymerizations were carried out with different ratios of monomer to initiator (see SI). Kinetic studies of each ratio of monomer to initiator were completed before each sample was synthesized to determine the reaction time for the approximate desired molecular weight for each metallopolymer sample. After purification was completed, the resulting metallopolymer was furthered characterized by DOSY NMR, GPC, and IR to establish the size and molecular weight (See SI). The samples were stored under Ar at -20°C. The samples retained their catalytic activity for over 2 years even after repeated warming to room temperature and exposure to oxygen during sampling and experimentation. 13,23-25

Scheme 1. Synthetic scheme for PDMAEMA-*g*-[2Fe-2S] metallopolymers of different sizes.

Example reaction conditions for polymer chain lengths n:

A:B = 1:50 1 hour $n \approx 9$ **A:B** = 1:100 $\frac{1}{2}$ hour $n \approx 36$ **A:B** = 1:200 2 hours $n \approx 11$

Hydrodynamic radii of the metallopolymers. The most important feature of the size of the metallopolymers in relation to these experiments is the geometric dimension of the metallopolymer rather than the molecular weight. Therefore, the metallopolymers discussed in this study will be delineated based on the hydrodynamic radii. The hydrodynamic radii of the metallopolymers were estimated experimentally from the diffusion coefficients measured by ¹H DOSY NMR and the Stokes-Einstein equation. The ¹H DOSY NMR were performed in 1 M TRIS-DCl in D2O adjusted to a pH of 7.00 ± 0.01 to have a metric of metallopolymer size in the same solution conditions that were employed for the electrocatalytic analysis. The ¹H DOSY measurement gives reproducible diffusion coefficients with an uncertainty of approximately 1%. The Stokes-Einstein equation assumes that the object is spherical, however, PDMAEMA-g-[2Fe-2S] metallopolymers are likely not spherical as shown by the model in Figure 2.24 The ratio of equatorial (a) and axial (c) radii is less than three for these metallopolymer systems which corresponds to an over-approximation of the Stokes radii by $\sim 10\%$. For this study, analyses of PDMAEMA-q-[2Fe-2S] metallopolymers with the approximate hydrodynamic radii of 18 Å, 28Å, 42 Å and 64 Å (see equation S.1) are discussed.

Cyclic voltammetry comparison. The electrocatalytic production of hydrogen by PDMAEMA-g-[2Fe-2S] metallopolymers with different hydrodynamic radii were investigated by CV in neutral solution with 1 M TRIS used as a protic buffer electrolyte¹⁸ (Figure 3). The H₂ generation by the PDMAEMA-g-[2Fe-2S] metallopolymers showed an increase in catalytic current density with decrease in hydrodynamic radii from 64 Å to 18 Å. The peak current density of the small metallopolymer was attenuated by rapid H₂ bubble formation at the electrode and can be seen in the unusual CV profile as the scan proceeds through the peak. The average peak current densities of multiple CVs taken at 0.1 V/s for the 18 Å metallopolymer was -92 ± 10 mA/cm², -84 $\pm 4 \text{ mA/cm}^2$ for the 42 Å, and $-62 \pm 11 \text{ mA/cm}^2$ for the 64 Å. The standard deviations are a consequence of variations in surface conditions for adsorption and bubble formation from experiment to experiment.

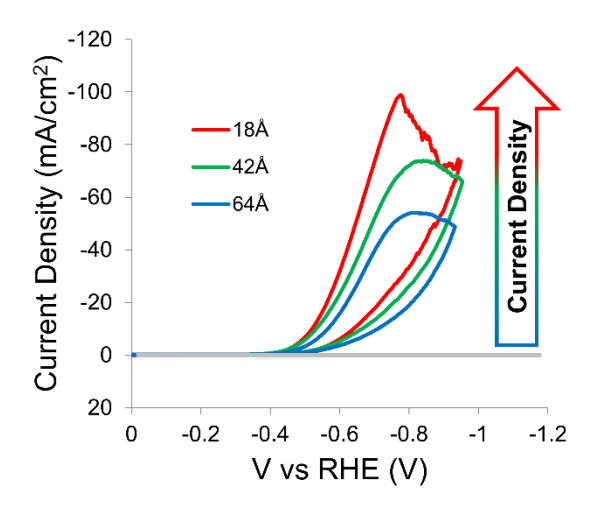


Figure 3. Cyclic voltammetry comparison of PDMAEMA–g–[2Fe–2S] metallopolymers with hydrodynamic radii of 18 Å (red), 42 Å (green), 64 Å (blue), and glassy carbon (grey) in 1 M TRIS adjusted to pH 7.00 \pm 0.01 aqueous solution. Experiments were conducted at a scan rate of 0.10 V/s.

Metallopolymer concentration dependence. Figure 4 shows the dependence of current density on concentration of the metallopolymers based on CVs taken at 0.10 V/s. The concentration dependence follows the form of a Langmuir adsorption isotherm. The plateau of the current density beginning around a concentration of 1 μ M is due to formation of a monolayer of the metallopolymers on the surface. The dashed lines in Figure 4 show fits of the adsorption isotherms using a standard Langmuir model. In the Langmuir adsorption model, the current density j is given by a maximum current density j_{max} times the fraction of adsorption sites occupied (θ) by an electroactive molecule (A):

$$j = j_{max} \times \theta = j_{max} \times \frac{K_{ads}[A]}{1 + K_{ads}[A]}$$
 Equation 1

where K_{ads} is the equilibrium constant for adsorption characterized by the reaction:

$$A + S \rightleftharpoons AS$$
 Equation 2

In Equation 2, S is an empty surface site and AS is a site on the electrode occupied by A. The fits are generated by optimizing the two parameters j_{max} and K_{ads} of Equation 1 for a range of [A] values. The j_{max} values increase from 52 mA/cm² for the 64 Å metallopolymer to 72 mA/cm² for the 42 Å metallopolymer to 87 mA/cm² for the 18 Å metallopolymer, indicative of an increasing number of electroactive species in a monolayer on the surface with decreasing size of the species. The equilibrium constants for adsorption (K_{ads}) used in the fits shown in Figure 4 were $K_{ads} = 13$ for the 18 Å, $K_{ads} = 8$ for the 42 Å, and $K_{ads} = 5$ for the 64 Å. The observed increase of K_{ads} with the decrease of polymer size is consistent with less steric crowding and more available adsorption sites for the smaller polymers per unit area.

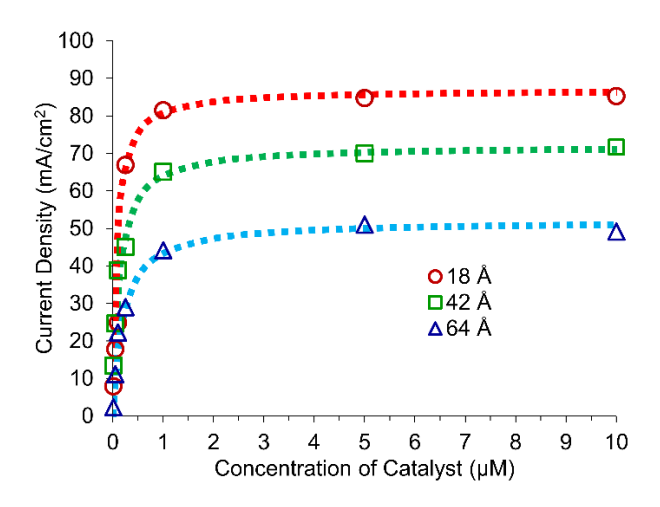


Figure 4. Current density versus concentration comparison for PDMAEMA–g–[2Fe–2S] metallopolymers with hydrodynamic radii of 18 Å (red circles), 42 Å (green squares), and 64 Å (blue triangles) in 1 M TRIS adjusted to pH 7.00 \pm 0.01. The dashed lines show fits of the adsorption isotherm with a Langmuir model. Experiments were performed with a glassy carbon electrode and a scan rate of 0.10 V/s.

The adsorption on the surface persists after completion of the electrochemical experiments and removal of the electrode from the solution. After removing and rinsing the electrode and then placing the electrode in a solution with the same electrolyte but not containing metallopolymer, the first CV scan shows the same catalytic peak with the current density reduced by 15-50%. The catalysis peak disappears on subsequent scans, consistent with the transient equilibrium nature of the adsorption indicated by the Langmuir isotherms. ¹⁸

Electrochemically active surface coverage (ECSC). The different sizes of the polymers as indicated by the hydrodynamic radii leads to different amounts of electroactive [2Fe-2S] catalyst adsorbed to the electrode. The electrochemically active surface coverage (ECSC, sites per square centimeter) for each metallopolymer size was evaluated using the current of the pre-catalytic reduction of the [2Fe-2S] active site (Figure 5). To measure this precatalytic reduction, the CVs were performed in 1 M TRIS adjusted to pH 8.00 ± 0.01. By changing to a higher pH solution, the thermodynamic potential of catalysis is shifted more negative allowing for the initial reduction of [2Fe-2S] to be observed before the catalytic peak. With observation of these pre-catalytic currents due to reduction of the active site, the ECSC can be estimated using Equation 3.27 The initial reduction currents were found to be $-0.22~\mu A$ for the 28 Å, $-0.16~\mu A$ for the 42 Å, and -0.08 μA for the 64 Å. The amount of electroactive [2Fe-2S] sites absorbed to the cathode was estimated to be 8.2 x 10⁻¹² mol/cm² for the 28 Å radius sample, $6.0 \times 10^{-12} \text{ mol/cm}^2 \text{ for } 42 \text{ Å, and } 3.0 \times 10^{-12} \text{ mol/cm}^2 \text{ for } 64$ Å. The results are summarized in Table S2 in the SI. An overall increase in [2Fe-2S] catalyst ECSC trends with reducing the polymer size.

$$\Gamma_{echem} = \frac{i_{[2Fe-2S]}}{\left(n^2F^2/_{4RT}\right)vA}$$
 Equation 3

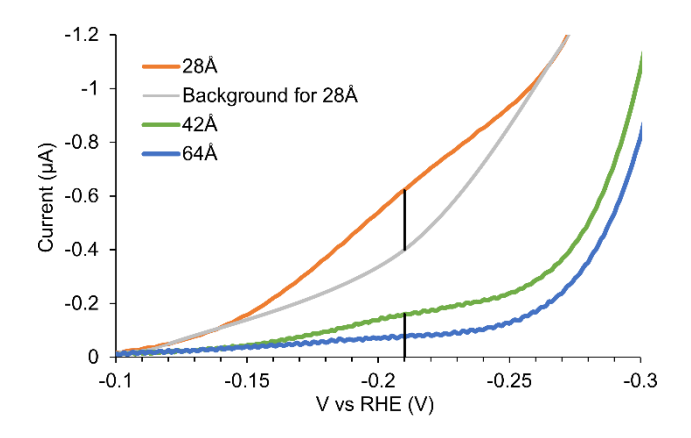


Figure 5. CVs in 1.00 M TRIS adjusted to pH 8.00 \pm 0.01 of the initial reduction of the [2Fe–2S] active site with a concentration of 10 μ M metallopolymer with hydrodynamic radii of 28 Å (orange), 42 Å (green), and 64 Å (blue) PDMAEMA–g–[2Fe–2S] metallopolymer. The CVs are adjusted for a linear baseline. The grey trace shows the rise of catalytic current for the 28 Å sample. The peak currents of the pre-catalytic reduction were estimated at -2.1 V as shown by the black vertical lines.

The concentration of metallopolymers in a monolayer on the surface can be estimated with a simple physical model based on the area of the surface occupied by the metallopolymer (similar to that shown in Figure 2). The close-packed concentrations are very similar to the electrochemically active surface concentrations (see Table S2). This agreement indicates that the metallopolymers form reasonably close-packed arrangements on the surface and all of the adsorbed [2Fe–2S] sites are electrochemically active. This is an important finding in explaining the high activity of these metallopolymer electrocatalysts because it demonstrates an efficient and effective natural assembly of the metallopolymers and the [2Fe–2S] sites on the electrode surface.

Overpotential differences using linear sweep voltammetry. To illustrate the effect of polymer size on overpotential, linear sweep voltammetry was performed with a rotating disk electrode. Shown in Figure 6, the onset of catalytic current occurs at approximately -0.45 V for all three metallopolymer sizes. This indicates that the electron transfer overpotential for onset of current is independent of polymer size, consistent with the similar proximity of the active sites to the electrode surface. The similarity of onset potential for catalysis also indicates that the thermodynamic and reaction overpotentials are similar. The overpotentials diverge when scanned to more negative potentials for higher current densities. Comparison of overpotentials at a current density of 10 mA/cm² is common in the literature (often referred to as η_{10}).²⁸ The overpotential change between the large and small metallopolymers of 22 mV to reach a current density of 10 mA/cm² is attributed to a difference in concentration overpotential for the surface concentration of the catalyst. The larger metallopolymer has a larger concentration overpotential because of the smaller concentration of active sites on the surface. Consequently, the larger metallopolymer requires a more negative potential to reach the same current density as the smaller metallopolymer. The difference in concentration overpotential increases as the current density increases. A summary of the polymer sizes and electrochemical characteristics is given in Table 1.

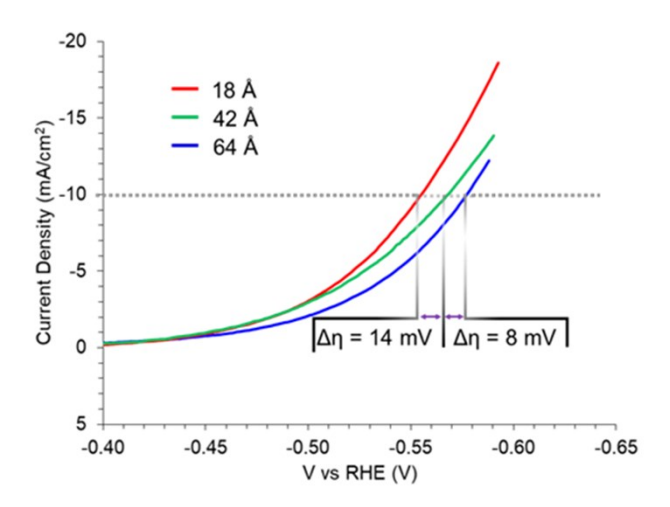


Figure 6. Linear sweep voltammograms of 10 μM PDMAEMA-g–[2Fe–2S] metallopolymers with hydrodynamic radii of 18 Å (red), 42 Å (green), and 64 Å (blue) using a rotating disk electrode at a rotation of 2000 RPM and scan rate of 5 mV/s. Overpotentials are indicated at current densities of 10 mA/cm² (grey dashed line) with change in overpotential (Δη) indicated.

Table 1. Summary of metallopolymer size and electrocatalytic characteristics.

$M_{n,GPC}$ (g/mol)	R _{hyd} ^a (Å)	J _{@0.10 V/s} b (mA/cm ²)	η^c_{10} (V)
3.5k	18	-92 ± 10	-0.56
12.2k	42	-84 ± 4	-0.57
24.3k	64	-62 ± 11	-0.58

 $[^]a$ 1H DOSY NMR was performed in 1 M TRIS-DCl in D2O with a metallopolymer concentration of approximately 100 μM

Rate of catalysis. Due to the fast rate for catalysis observed for the PDMAEMA-*g*-[2Fe-2S] metallopolymers, the proton source near the electrode is rapidly depleted during a CV performed at a scan rate of 0.1 V/s and bubble formation becomes problematic. Both factors are rate limiting. To diminish the effect of proton source depletion and bubble formation, CVs were taken with increasing scan rates to decrease the time scale of the experiment to the point where current density is no longer dependent on scan rate.²⁹ As shown in Figure 7, the catalytic current density becomes independent of the scan rates when the CVs are swept at a rate of 8.1 V/s and higher. The average current densities for the three measurements in the plateau region were found to be -621 mA/cm² for the 28 Å, -437 mA/cm² for the 42 Å, and -234 mA/cm² for the 64 Å metallopolymer.

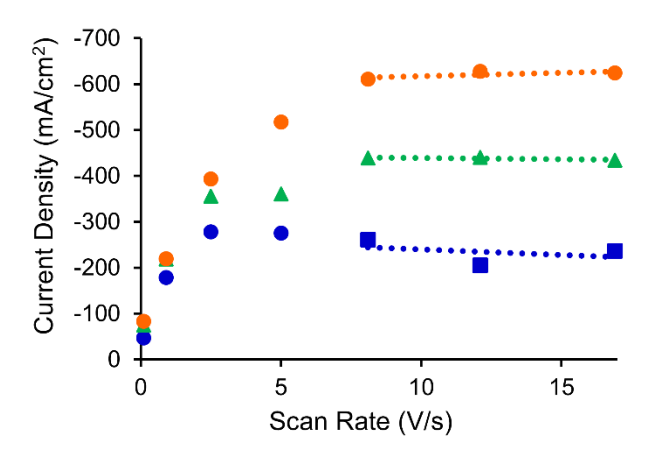


Figure 7. Dependence of current density on scan rate for PDMAEMA-g-[2Fe-2S] metallopolymers with hydrodynamic radii of 28 (orange circles), 42 (green triangles), and 64 Å (blue squares) in 1 M TRIS adjusted to pH 7.00 ± 0.01 .

Catalytic rates. Using these plateau current densities (J_{pl}), in conjunction with the estimated surface coverage determined above, the catalytic rates of hydrogen molecule production per active site per second can be approximated. The per-active site rates (~ $\pm5\%$) were found to be 3.9×10^5 s⁻¹ for the 28 Å, 3.8×10^5 s⁻¹ for the 42 Å, and 4.1×10^5 s⁻¹ for the 64 Å. The rates of hydrogen production per active site do not trend with polymer size indicating that the polymer corona is not inhibiting proton transfer to the [2Fe-2S] active site.

Table 2. Experimental polymer and electrocatalytic characteristics for plateau current and rate of active site.

$M_{n,GPC}$ (g/mol)	R _{hyd} , ^a (Å)	J _{pl} ^b (mA/cm ²)	$\Gamma_{\rm echem}$ (mol/cm ²)	k ^c (s ⁻¹)
8.5k	28	-621	8.2×10 ⁻¹²	3.9×10 ⁵
12.2k	42	-437	6.0×10 ⁻¹²	3.8×10 ⁵
24.3k	64	-234	3.0×10 ⁻¹²	4.1×10 ⁵

 $^{^{\}rm a~1H}$ DOSY NMR was performed in 1 M TRIS-DCl in D_2O with a metallopolymer concentration of approximately 100 $\mu M.$

Electrochemical impedance spectroscopy (EIS) to compare resistance to electron transfer in catalysis. Electrochemical impedance spectroscopy also shows that the performance of the catalytic site is not strongly dependent on the size of the metallopolymer. Nyquist plots from the EIS of three different-sized metallopolymers are shown in Figure 8. The holding potential is in the region of catalysis slightly above 10 mA/cm² current density (Figure 6). The Nyquist plots show that a single overall time-constant

 $^{^{\}text{b}}$ Cyclic voltammetry peak current density. The peak current density of the small metallopolymer was attenuated by rapid H_2 bubble formation at the electrode.

 $^{^{\}rm c}$ Overpotential vs, RHE at current density of 10 mA/cm² was determined using LSV (scan rate of 5 mV/s) with a rotating disk electrode (2000 RPM).

 $^{^{\}rm b}$ Plateau current densities are an average of current densities from scan rates of 8.1, 12.1, and 16.9 V/s at –0.9 V vs RHE (see Figure 7).

 $^{^{\}rm c}$ Rate of hydrogen molecules produced per catalytic site per second at the plateau current.

feature dominates catalysis. The EIS data does not show evidence of a Warburg impedance indicating that a diffusioncontrolled process is not a significant factor. The simple standard equivalent circuit shown in Figure 8d models the EIS data well. The circuit has a commonly used resistor/capacitor (RC) combination preceded by the uncompensated resistance (Ru) of the system. The capacitor of the RC circuit is a constant phase element typically used to account for the imperfect capacitance seen with an electrochemical double layer.³⁰ The alpha value for capacitance is close to 0.9 in each case. The fits of the EIS Nyquist plots show only minor differences in the resistance to charge transfer with 53 Ω for 18 Å, 51 Ω for the 42 Å, and 47 Ω for the 64 Å metallopolymer. The differences are due primarily to small differences in low frequency impedance on the right of the Nyquist curves related to the adsorption of the metallopolymers.31 These differences are most clearly seen in the low-frequency region of the Bode plots (Figure S15). The smaller metallopolymers show evidence at low frequencies of a second high-resistance process that contributes a small amount to catalysis, and the largest metallopolymer shows evidence of an inductive component at low frequencies. Overall, the EIS data demonstrates that the electroactive [2Fe-2S] sites adsorbed to the surface have similar charge transfer resistances, meaning they have similar electron transfer rates and similar proton reduction rates.³² Increasing polymer size does not inhibit the rate of electron transfer in catalysis appreciably, indicating the [2Fe-2S] active sites are in similar contact with the electrode and solution.

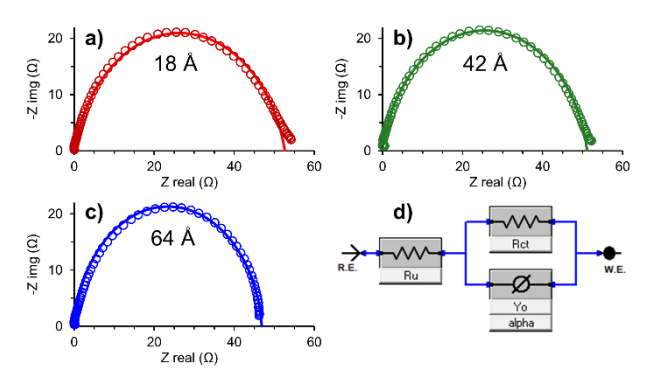


Figure 8. EIS comparison of metallopolymers with hydrodynamic radii of a) 18 Å (red), b) 42 Å (green), and c) 64 Å (blue). Experimental data are open circles and fits are solid lines. The equivalent circuit used for all fits is shown in d). The EIS data was collected using a RDE rotating at 2000 RPMs with 10 mV of alternating current at a holding potential of –0.59 V vs RHE (see SI).

Molecular dynamics. To further corroborate and provide additional insight into the metallopolymer-electrode surface conformational dynamics, an initial molecular dynamics (MD) modeling of the adsorption of the metallopolymer to the electrode surface was carried out. Details are in the SI. Snapshots of intermediate steps in the adsorption dynamics are illustrated in Figure 9 and a video of the entire adsorption process is included with the SI. After dynamics sampling of the conformer structures of the 3.5k molecular weight metallopolymer and annealing the structure, the metallopolymer was placed ~5Å above a slightly negatively charged graphite surface (~0.0003 e- per carbon atom) as

shown in Figure S16. With initiation of the dynamics, the protonated amines are drawn directly to the cathode surface by electrostatic forces as shown in Figure 9a after $\sim\!2$ picoseconds. After $\sim\!10$ picoseconds the protonated amines of the polymer arms on both sides of the active site are adsorbed to the surface. The polymer continues to spread and flatten against the surface and within less than 20 picoseconds this action pulls the active site into close contact with the surface as shown in Figure 9b. The retention of the active site close to the surface is conducive to fast electron transfer.

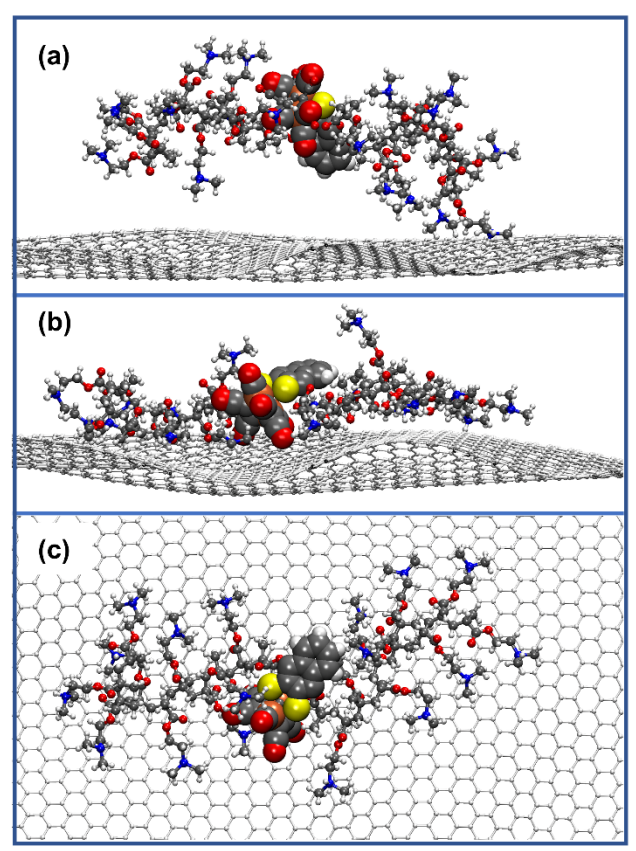


Figure 9. Snapshots of the molecular dynamics simulation of adsorption of the 3.5 kDa PDMAEMA-*g*-[2Fe-2S] metallopolymer on a graphite surface. The active site is depicted with van der Waals radii and the polymer is depicted as balls and sticks. (a) adsorption begins as protonated amines are pulled to the surface (~2 picoseconds), (b) protonated amines complete adsorption of the metallopolymer to the surface and position the active site close to the surface for electron transfer (<20 picoseconds), (c) view looking down at the surface of the adsorbed metallopolymer showing the spread of the protonated amine tethers to the surface and the accessibility of the active site to protonation.

Looking down on the fully adsorbed species on the surface in Figure 9c shows the protonated amines spread out to tether the metallopolymer to the surface. This view also shows that the sulfur atoms and one iron atom are exposed to solution. These are the sites proposed for protonation in catalytic schemes of proton reduction by hydrogenases and their mimics.^{33,34} In addition to the geometric accessibility of these sites, the two-electron reduced active site³⁵ has a strong electrostatic attraction for protons and fast proton transfer. This positioning of the active site next to the

surface will occur similarly for the longer polymers, so the electron transfer rates and proton reduction rates per active site will be similar as observed.

The molecular dynamics also show that the metallopolymer has little barrier to gliding over the surface, and thus the metallopolymers can adjust to a close-packing arrangement. The smaller metallopolymer has a greater current per unit area simply because it has more active sites per unit area in a close-packed arrangement. Finally, a second layer of metallopolymer does not have the benefit of the protonated amines interacting directly with the electrode surface, and in contrast has repulsive interactions between with the protonated amines in the first monolayer. The Langmuir plots in Figure 4 show that a second layer of metallopolymers is not favored at these concentrations, so the active sites are not covered and remain exposed to the solution.

3. CONCLUSIONS

Incorporation of the electrocatalytic active site into the PDMAEMA metallopolymer enhances the rate and lowers the overpotential for reduction of protons to hydrogen in water. Smaller PDMAEMA-g-[2Fe-2S] metallopolymers exhibit larger current densities and lower concentration overpotentials when compared to their larger analogues. This is a consequence of more electroactive [2Fe-2S] active sites adsorbed per unit surface area of the electrode for the smaller metallopolymers. This study finds that the per-active site rate of catalysis and electron transfer rates are similar across the different sized metallopolymers. Those factors are a consequence of the similar positioning of the [2Fe-2S] active site with respect to the surface and to bulk solution regardless of the polymer size. Molecular dynamics simulations of the adsorption process reveal an electrostatic attraction of the protonated amines to the electrode surface that spreads the metallopolymer to a mostly twodimensional structure on the surface that pulls one side of the active site to close proximity to the electrode for fast electron transfer and leaves the other side of the active site exposed to solution. The high negative charge of the reduced active site is conducive to fast proton transfer to the site and reduction. The mobility of the metallopolymer to slide across the surface and pack into a tight, self-assembled monolayer leads to the high current per geometric surface area of the electrode. Other catalysts for reductive reactions, such as catalysts for carbon dioxide or nitrogen reduction, should also benefit from the natural assembly of PDMAEMA metallopolymers on the electrode surface to position the electrocatalyst for fast electron transfer and open interaction with the bulk solution.

ASSOCIATED CONTENT

Supplemental Information.

Materials and methods for sample preparations, characterizations, electrochemistry, and molecular dynamics for polymer modeling and adsorption. Additional supporting spectral and electrochemical data. Video of the molecular dynamics adsorption. This material is available free of charge via the Internet at http://pubs.acs.org.

AUTHOR INFORMATION

Corresponding Author

* E-mail: <u>dlichten@arizona.edu</u> * E-mail: <u>rglass@arizona.edu</u> * E-mail: jpyun@arizona.edu

ORCID

Dennis L. Lichtenberger: 0000-0002-9271-0311

Jeffrey Pyun: 0000-0002-1288-8989

Author Contributions

The manuscript was written through contributions of all authors. / All authors have given approval to the final version of the manuscript. / ‡These authors contributed equally.

Funding Sources

DLL, RSG, and JP gratefully acknowledge support of this work by NSF (awards CHE-1664745 and CHE-1954641).

Notes

The authors declare no competing financial interest.

ACKNOWLEDGMENT

DLL, JP, and RSG gratefully acknowledge NSF (awards CHE-166745 and CHE-1954641) for the support of this work and Krzysztof Matyjaszewski and Tong Liu for their assistance with gel permeation chromatography analysis.

ABBREVIATIONS

HER, hydrogen evolution reaction; DMAEMA, (2-dimethyl amino)ethyl methacrylate; ATRP, atom transfer radical polymerization, CV, cyclic voltammetry; LSV, linear sweep voltammetry; EIS, electronic impedance spectroscopy; ECSC, electrochemically active surface coverage; GPC, gel permeation chromatography; pdt, propanedithiolate;

REFERENCES

- (1) Markovic, N. M. Electrocatalysis: Interfacing Electrochemistry. *Nat. Mater.* **2013**, *12* (2), 101–102. https://doi.org/10.1038/nmat3554.
- (2) O'Mullane, A. P.; Escudero-Escribano, M.; Stephens, I. E. L.; Krischer, K. The Role of Electrocatalysis in a Sustainable Future: From Renewable Energy Conversion and Storage to Emerging Reactions. *ChemPhysChem* **2019**, 20 (22), 2900–2903. https://doi.org/10.1002/cphc.201901058.
- (3) Xu, Z. J.; Wang, X. Electrocatalysis: A Core Technique for a Sustainable Future. *Chemistry–Eur. J.* **2020**, *26* (18), 3897. https://doi.org/https://doi.org/10.1002/chem.2020009

https://doi.org/https://doi.org/10.1002/chem.2020009

- (4) Novaes, L. F. T.; Liu, J.; Shen, Y.; Lu, L.; Meinhardt, J. M.; Lin, S. Electrocatalysis as an Enabling Technology for Organic Synthesis. *Chem. Soc. Rev.* **2021**, *50* (14), 7941–8002. https://doi.org/10.1039/d1cs00223f.
- (5) Roger, I.; Shipman, M. A.; Symes, M. D. Earth-Abundant Catalysts for Electrochemical and Photoelectrochemical Water Splitting. *Nat. Rev. Chem.* **2017**, *1*, 0003. https://doi.org/10.1038/s41570-016-0003.
- (6) Faber, M. S.; Jin, S. Earth-Abundant Inorganic Electrocatalysts and Their Nanostructures for Energy

- Conversion Applications. *Energy Environ. Sci.* **2014**, *7* (11), 3519–3542. https://doi.org/10.1039/c4ee01760a.
- (7) Gao, S.; Fan, W.; Liu, Y.; Jiang, D.; Duan, Q. Artificial Water-Soluble Systems Inspired by [FeFe]-Hydrogenases for Electro- and Photocatalytic Hydrogen Production. *Int. J. Hydrogen Energy* **2020**, *45* (7), 4305–4327. https://doi.org/10.1016/j.ijhydene.2019.11.206.
- (8) Simmons, T. R.; Berggren, G.; Bacchi, M.; Fontecave, M.; Artero, V. Mimicking Hydrogenases: From Biomimetics to Artificial Enzymes. *Coord. Chem. Rev.* **2014**, *270–271* (1), 127–150. https://doi.org/10.1016/j.ccr.2013.12.018.
- (9) Ahmed, M. E.; Dey, A. Recent Developments in Bioinspired Modelling of [NiFe]- and [FeFe]-Hydrogenases. *Curr. Opin. Electrochem.* **2019**, *15*, 155–164. https://doi.org/10.1016/J.coelec.2019.05.009.
- (10) Kleinhaus, J. T.; Wittkamp, F.; Yadav, S.; Siegmund, D.; Apfel, U. P. [FeFe]-Hydrogenases: Maturation and Reactivity of Enzymatic Systems and Overview of Biomimetic Models. *Chem. Soc. Rev.* **2021**, *50* (3), 1668–1784. https://doi.org/10.1039/D0CS01089H.
- (11) Wang, M.; Chen, L.; Sun, L. Recent Progress in Electrochemical Hydrogen Production with Earth-Abundant Metal Complexes as Catalysts. *Energy Environ. Sci.* **2012**, 5 (5), 6763–6778. https://doi.org/10.1039/c2ee03309g.
- (12) Wang, V. C. C.; Esmieu, C.; Redman, H. J.; Berggren, G.; Hammarström, L. The Reactivity of Molecular Oxygen and Reactive Oxygen Species with [FeFe] Hydrogenase Biomimetics: Reversibility and the Role of the Second Coordination Sphere. *Dalton Trans.* **2020**, *49* (3), 858–865. https://doi.org/10.1039/C9DT04618F.
- (13) Brezinski, W. P.; Karayilan, M.; Clary, K. E.; Pavlopoulos, N. G.; Li, S.; Fu, L.; Matyjaszewski, K.; Evans, D. H.; Glass, R. S.; Lichtenberger, D. L.; Pyun, J. [FeFe]-Hydrogenase Mimetic Metallopolymers with Enhanced Catalytic Activity for Hydrogen Production in Water. *Angew. Chem. Int. Ed.* **2018**, *57* (37), 11898–11902. https://doi.org/10.1002/anie.201804661.
- (14) Brezinski, W. P.; Karayilan, M.; Clary, K. E.; McCleary-Petersen, K. C.; Fu, L.; Matyjaszewski, K.; Evans, D. H.; Lichtenberger, D. L.; Glass, R. S.; Pyun, J. Macromolecular Engineering of the Outer Coordination Sphere of [2Fe-2S] Metallopolymers to Enhance Catalytic Activity for H₂ Production. *ACS Macro Lett.* **2018**, *7* (11), 1383–1387. https://doi.org/10.1021/acsmacrolett.8b00765.
- (15) Karayilan, M.; Brezinski, W. P.; Clary, K. E.; Lichtenberger, D. L.; Glass, R. S.; Pyun, J. Catalytic Metallopolymers from [2Fe-2S] Clusters: Artificial Metalloenzymes for Hydrogen Production. *Angew. Chem. Int. Ed.* **2019**, *58* (23), 7537–7550. https://doi.org/10.1002/anie.201813776.
- (16) Winkler, M.; Esselborn, J.; Happe, T. Molecular Basis of [FeFe]-Hydrogenase Function: An Insight into the Complex Interplay between Protein and Catalytic Cofactor. *Biochim Biophys Acta Bioenerg* **2013**, *1827* (8–9), 974–985. https://doi.org/10.1016/J.bbabio.2013.03.004. (17) In-noi, O.; Haller, K. J.; Hall, G. B.; Brezinski, W. P.; Marx, J. M.; Sakamoto, T.; Evans, D. H.; Glass, R. S.; Lichtenberger, D. L. Electrochemical, Spectroscopic, and Computational Study of Bis(μ-Methylthiolato)Diironhexacarbonyl: Homoassociative Stabilization of the Dianion and a Chemically Reversible Reduction/Reoxidation Cycle. *Organometallics* **2014**, *33* (18), 5009–5019. https://doi.org/10.1021/om5004122.
- (18) Clary, K. E.; Karayilan, M.; McCleary-Petersen, K. C.; Petersen, H. A.; Glass, R. S.; Pyun, J.; Lichtenberger, D. L. Increasing the Rate of the Hydrogen Evolution Reaction in Neutral Water with Protic Buffer Electrolytes. *Proc.*

- *Natl. Acad. Sci. U.S.A.* **2021**, *117* (52), 32947–32953. https://doi.org/10.1073/PNAS.2012085117.
- (19) Vincent, K. A.; Parkin, A.; Armstrong, F. A. Investigating and Exploiting the Electrocatalytic Properties of Hydrogenases. *Chem. Rev.* **2007**, *107* (10), 4366–4413. https://doi.org/10.1021/cr050191u [doi].
- (20) Madden, C.; Vaughn, M. D.; Diez-Perez, I.; Brown, K. A.; King, P. W.; Gust, D.; Moore, A. L.; Moore, T. A. Catalytic Turnover of FeFe]-Hydrogenase Based on Single-Molecule Imaging. *J. Am. Chem. Soc.* **2012**, *134* (3), 1577–1582. https://doi.org/10.1021/ja207461t.
- (21) Hatchikian, E. C.; Forget, N.; Fernandez, V. M.; Williams, R.; Cammack, R. Further Characterization of the [Fe]-Hydrogenase from Desulfovibrio Desulfuricans ATCC 7757. *Eur. J. Biochem.* **1992**, *209* (1), 357–365.
- (22) Karayilan, M.; McCleary-Petersen, K. C.; Hamilton, M. O.; Fu, L.; Matyjaszewski, K.; Glass, R. S.; Lichtenberger, D. L.; Pyun, J. Synthesis of Metallopolymers via Atom Transfer Radical Polymerization from a [2Fe-2S] Metalloinitiator: Molecular Weight Effects on Electrocatalytic Hydrogen Production. *Macromol. Rapid Commun.* **2020**, 41 (1), 1900424. https://doi.org/10.1002/marc.201900424.
- (23) Ahmed, M. E.; Dey, S.; Darensbourg, M. Y.; Dey, A. Oxygen-Tolerant H₂ Production by [FeFe]-H₂Ase Active Site Mimics Aided by Second Sphere Proton Shuttle. *J. Am. Chem. Soc.* **2018**, *140* (39), 12457–12468. https://doi.org/10.1021/jacs.8b05983.
- (24) Mondal, B.; Dey, A. Development of Air-Stable Hydrogen Evolution Catalysts. *Chem. Commun.* **2017**, *53* (53), 7707–7715. https://doi.org/10.1039/c7cc02941a.
- (25) Winkler, M.; Duan, J.; Rutz, A.; Felbek, C.; Scholtysek, L.; Lampret, O.; Jaenecke, J.; Apfel, U. P.; Gilardi, G.; Valetti, F.; Fourmond, V.; Hofmann, E.; Léger, C.; Happe, T. A Safety Cap Protects Hydrogenase from Oxygen Attack. *Nat. Commun.* **2021**, *12* (1), 1–10. https://doi.org/10.1038/s41467-020-20861-2.
- (26) Macchioni, A.; Ciancaleoni, G.; Zuccaccia, C.; Zuccaccia, D. Determining Accurate Molecular Sizes in Solution through NMR Diffusion Spectroscopy. *Chem. Soc. Rev.* **2008**, *37* (3), 479–489. https://doi.org/10.1039/B615067P.
- (27) Prodromidis, M.; Florou, A.; Tzouwara-Karayanni, S.; Karayannis, M. The Importance of Surface Coverage in the Electrochemical Study of Chemically Modified Electrodes. *Electroanal.* **2000**, *12*, 1498–1501. https://doi.org/10.1002/1521-4109(200012)12:183.0.CO;2-Y.
- (28) Hansen, J. N.; Prats, H.; Toudahl, K. K.; Mørch Secher, N.; Chan, K.; Kibsgaard, J.; Chorkendorff, I. Is There Anything Better than Pt for HER? *ACS Energy Lett.* **2021**, 6 (4), 1175–1180. https://doi.org/10.1021/acsenergylett.1c00246.
- (29) Rountree, E. S.; McCarthy, B. D.; Eisenhart, T. T.; Dempsey, J. L. Evaluation of Homogeneous Electrocatalysts by Cyclic Voltammetry. *Inorg. Chem.* **2014**, *53* (19), 9983–10002. https://doi.org/10.1021/ic500658x.
- (30) Cördoba-Torres, P.; Mesquita, T. J.; Nogueira, R. P. Relationship between the Origin of Constant-Phase Element Behavior in Electrochemical Impedance Spectroscopy and Electrode Surface Structure. *J. Phys. Chem. C* **2015**, 119 (8), 4136–4147. https://doi.org/10.1021/JP512063F.
- (31) Klotz, D. Negative Capacitance or Inductive Loop? A General Assessment of a Common Low Frequency Impedance Feature. *Electrochem. Commun.* **2019**, 98, 58–62.
- https://doi.org/10.1016/j.elecom.2018.11.017.

- (32) Bard, A. J.; Faulkner, L. R. *Electrochemical Methods: Fundamentals and Applications*, 2nd ed.; Harris, D., Swain, E., Aiello, E., Eds.; John Wiley & Sons, Inc: New York, 2001.
- (33) Jablonskyte, A.; Wright, J. A.; Pickett, C. J. Mechanistic Aspects of the Protonation of [FeFe]-Hydrogenase Subsite Analogues. *Dalton Trans.* **2010**, *39* (12), 3026–3034.
- (34) Schilter, D.; Camara, J. M.; Huynh, M. T.; Hammes-Schiffer, S.; Rauchfuss, T. B. Hydrogenase Enzymes and Their Synthetic Models: The Role of Metal Hydrides.
- Chem. Rev. 2016, 8693-8749. 116 (15),https://doi.org/10.1021/acs.chemrev.6b00180. Felton, G. A. N.; Vannucci, A. K.; Chen, J.; Lock-(35)ett, L. T.; Okumura, N.; Petro, B. J.; Zakai, U. I.; Evans, D. H.; Glass, R. S.; Lichtenberger, D. L. Hydrogen Generation from Weak Acids: Electrochemical and Computational Studies of a Diiron Hydrogenase Mimic. J. Am. Chem. Soc. 2007, 129 (41), 12521-12530. https://doi.org/10.1021/ja073886g.

Insert Table of Contents artwork here

